

1 **Nonhydrostatic Effects and the Determination of Icy Satellites' Moment of Inertia**

2

3 Peter Gao<sup>1,\*</sup> and David J. Stevenson<sup>1</sup>

4

5 *<sup>1</sup>Division of Geological and Planetary Sciences, California Institute of Technology, Pasadena, CA,*  
6 *USA, 91125*

7

8 *\*Corresponding author at: Division of Geological and Planetary Sciences, California Institute of*  
9 *Technology, Pasadena, CA, USA, 91125*

10 *Email address: [pgao@caltech.edu](mailto:pgao@caltech.edu)*

11 *Phone number: 626-298-9098*

12 **Abstract**

13 We compare the moment of inertia (MOI) of a simple hydrostatic, two layer body as determined by the  
14 Radau-Darwin Approximation (RDA) to its exact hydrostatic MOI calculated to first order in the  
15 parameter  $q = \Omega^2 R^3 / GM$ , where  $\Omega$ ,  $R$ , and  $M$  are the spin angular velocity, radius, and mass of the  
16 body, and  $G$  is the gravitational constant. We show that the RDA is in error by less than 1% for many  
17 configurations of core sizes and layer densities congruent with those of solid bodies in the Solar  
18 System. We then determine the error in the MOI of icy satellites calculated with the RDA due to  
19 nonhydrostatic effects by using a simple model in which the core and outer shell have slight degree 2  
20 distortions away from their expected hydrostatic shapes. Since the hydrostatic shape has an associated  
21 stress of order  $\rho \Omega^2 R^2$  (where  $\rho$  is density) it follows that the importance of nonhydrostatic effects scales  
22 with the dimensionless number  $\sigma / \rho \Omega^2 R^2$ , where  $\sigma$  is the nonhydrostatic stress. This highlights the likely  
23 importance of this error for slowly rotating bodies (e.g., Titan and Callisto) and small bodies (e.g.,  
24 Saturn moons other than Titan). We apply this model to Titan, Callisto, and Enceladus and find that the  
25 RDA-derived MOI can be 10% greater than the actual MOI for nonhydrostatic stresses as small as  $\sim 0.1$   
26 bars at the surface or  $\sim 1$  bar at the core-mantle boundary, but the actual nonhydrostatic stresses for a  
27 given shape change depends on the specifics of the interior model. When we apply this model to  
28 Ganymede we find that the stresses necessary to produce the same MOI errors as on Titan, Callisto, and  
29 Enceladus are an order of magnitude greater due to its faster rotation, so Ganymede may be the only  
30 instance where RDA is reliable. We argue that if satellites can reorient to the lowest energy state then  
31 RDA will always give an overestimate of the true MOI. Observations have shown that small  
32 nonhydrostatic gravity anomalies exist on Ganymede and Titan, at least at degree 3 and presumably  
33 higher. If these anomalies are indicative of the nonhydrostatic anomalies at degree 2 then these imply  
34 only a small correction to the MOI, even for Titan, but it is possible that the physical origin of  
35 nonhydrostatic degree 2 effects is different from the higher order terms. We conclude that

36 nonhydrostatic effects could be present to an extent that allows Callisto and Titan to be fully  
37 differentiated.

38

39 *Keywords:* Callisto; Enceladus; Ganymede; Interiors; Titan, interior

40 **1. INTRODUCTION**

41 Current models of icy satellite formation and evolution depend on the accuracy with which we  
42 determine their interior structures. These can be inferred from their moments of inertia (MOI), which  
43 can be estimated from *in situ* gravitational field measurements by spacecraft. The primary method of  
44 estimation is the Radau-Darwin approximation (RDA) (e.g., Hubbard 1984, Murray and Dermott  
45 1999), which relates the MOI to the degree 2 response of the body to rotation and tides expressed in the  
46 gravitational coefficients  $J_2$  and  $C_{22}$ , defined by:

47 
$$J_2 = \frac{C}{MR^2} - \frac{B+A}{2MR^2} \quad (1a)$$

48 
$$C_{22} = \frac{B-A}{4MR^2} \quad (1b)$$

49 where M and R are the mass and mean radius of the body, respectively; and  $C > B > A$  are the principle  
50 moments of inertia of the body. The accuracy of RDA for a two layer body has been explored in works  
51 such as Zharkov (2004) and Schubert et al. (2011), where the results of RDA are compared to the exact  
52 solution of Kong et al. (2010) and the results of the theory of figures, yielding relatively small  
53 differences of ~0.1%. The RDA makes three assumptions: (1) The body is in hydrostatic equilibrium;  
54 (2) there are no large density variations; (3) the perturbations arising from tides and rotation are small  
55 (i.e., linear response). Our primary focus here is on the first assumption. We note, however, that  
56 assumption (2) seems to have been insufficiently explored in the published literature and we  
57 accordingly have included brief consideration of this approximation here. Assumption (3) is violated  
58 for gas and ice giants because of their rapid rotation and this is the focus of the aforementioned theory  
59 of figures discussed in Hubbard (1984) and revisited very recently in Hubbard (2012) in the context of  
60 Maclaurin spheroids, the same approach that we use (in the linear limit).

61 The RDA has been used to determine the MOIs of several large icy satellites, such as Titan (Iess  
62 et al. 2010), Ganymede (Anderson et al. 1996), and Callisto (Anderson et al. 2001), as well as medium-  
63 sized satellites, such as Rhea (Iess et al. 2007). Enceladus is of great interest but no consensus has

64 emerged yet on the MOI for this body. Our main focus here is on the large icy bodies for which it is  
65 commonly assumed that RDA is accurate, but we will also briefly discuss the impact of RDA errors on  
66 Enceladus in anticipation of future results. Table 1 shows several physical and orbital parameters for  
67 these bodies, including their MOIs determined from RDA if available. Despite the similarities in the  
68 masses and radii of Titan, Ganymede, and Callisto, their determined moments of inertia appear to be  
69 vastly different: Ganymede's is low, implying full differentiation, while Titan and Callisto's are high,  
70 implying partial differentiation. This interpretation has influenced models for satellite formation such  
71 as the "gas-starved disk" model for the Galilean moons (Stevenson 2001; Canup and Ward 2002), and  
72 alternative ways of reducing accretion heating through lengthening the timescale of accretion (e.g.  
73 Mosqueira and Estrada, 2003). These models may avoid differentiation during accretion but  
74 differentiation may occur subsequently. In fact, the full differentiation of Ganymede is often attributed  
75 to later processes in this model such as tidal heating (Canup and Ward 2002), though differences in the  
76 formation environment such as a higher disk temperatures at Ganymede's orbital distance (Barr and  
77 Canup 2008) are also proposed. Some models avoid the full differentiation of Callisto and Titan due to  
78 later processes by constraining the formation times so as to avoid excessive heating by short-lived  
79 radioisotopes (Barr et al. 2010), while others allow for full differentiation of Titan but with a low-  
80 density, hydrated silicate core (Fortes 2012; Castillo-Rogez and Lunine 2010). Still others maintain that  
81 Callisto and Titan must fully differentiate in the lifetime of the Solar System due to density gradients  
82 trapping heat generated by long-lived radioisotopes (O'Rourke and Stevenson 2013).

83         Ultimately, the usefulness of these models depends on the accuracy of the MOIs that they  
84 attempt to explain, which in turn depends on the reliability of the RDA in determining the MOIs from  
85 the gravity measurements. The RDA predicts a one-to-one correspondence between MOI and  $J_2$  for a  
86 specific rotation, but nonhydrostatic effects destroy this correspondence by introducing a  
87 nonhydrostatic contribution to  $J_2$  that cannot be easily separated out from the measured  $J_2$  value. This

88 could be especially troublesome in slowly rotating bodies where the nonhydrostatic contribution could  
89 make up a large fraction of the total  $J_2$ , whereas the effect would be less in fast rotating bodies. For  
90 instance, Mueller and McKinnon (1988) noted that nonhydrostatic effects could be present on the slow  
91 rotator Callisto in magnitudes that would render its determined MOI untrustworthy. In this paper, we  
92 generalize this analysis to any degree 2 nonhydrostatic contribution and extend it to Titan and  
93 Ganymede, where long wavelength mass anomalies have been detected (Palguta et al. 2006; Iess et al.  
94 2010). This will allow us to both evaluate the accuracy of Titan and Callisto's determined MOIs given  
95 nonhydrostatic effects and determine whether Ganymede is less affected by these effects given its faster  
96 rotation. As previously mentioned, we will also extend our analysis to Enceladus due to its unique  
97 nature. Considering that a 10% error in the MOI of Callisto and a few % for Titan could potentially  
98 result in values consistent with fully differentiated bodies, it is essential that the effects of these  
99 nonhydrostatic structures be determined to establish their impact on the calculated MOIs of the large  
100 icy satellites, and in turn our understanding of their interiors and evolutionary processes.

101 In section 2, we first establish the error in RDA assuming exact hydrostatic equilibrium but  
102 allowing for large density differences in the context of a nested Maclaurin spheroid model. We then  
103 quantify the effects degree 2 nonhydrostatic anomalies have on the MOI of a generalized large icy  
104 satellite as determined by the RDA, as well as the relationship between the magnitude of the  
105 nonhydrostatic anomaly and the stress caused by such an anomaly on the icy satellite. In section 3 we  
106 apply our model to Titan, Ganymede, Callisto, and Enceladus and assess whether existing  
107 nonhydrostatic contributions and/or other possible sources are capable of producing major MOI errors.  
108 Finally, we summarize our work and state our conclusions in section 4.

109

## 110 **2. THEORY**

### 111 *2.1. Hydrostatic Icy Satellite Model*

112 The RDA can be expressed as

113 
$$\frac{C}{MR^2} = \frac{2}{3} \left( 1 - \frac{2}{5} \sqrt{\frac{5}{3\Lambda_{2,0} + 1} - 1} \right) \quad (2)$$

114 where  $C/MR^2$  is the nondimensionalized polar moment of inertia (Hubbard 1984). For a body deformed  
115 only by rotation  $\Lambda_{2,0} = J_2/q$  in the limit of small values of  $q$ , and

116 
$$q = \frac{\Omega^2 R^3}{GM} \quad (3)$$

117 is a dimensionless measure of the “centrifugal potential” that arise due to rotation, with  $\Omega$ ,  $R$ , and  $M$  as  
118 the spin angular velocity, mean radius, and mass of the body, and  $G$  as the gravitational constant. For  
119 synchronously rotating satellites, the tidal potential is three times the rotational potential in peak  
120 amplitude and this means that  $\Lambda_{2,0}$  is replaced by  $2J_2/5q$  (or equivalently  $\Lambda_{2,0}$  can be replaced in  
121 equation 2 by  $4C_{22}/3q$  ; note that this implies  $J_2/C_{22}=10/3$ ). But since we are dealing with linear theory  
122 it suffices to consider just the rotational disturbance; generalization to include the permanent tide is  
123 trivial. In order to simplify calculations and isolate the essential physics of the problem, we will  
124 consider a simple rotating two-layer icy satellite model with an ice mantle of constant density  $\rho_o$   
125 overlying a rocky core with constant density  $\rho_c$ . In comparison to real icy satellites, our model ice  
126 mantle includes the outer ice shell and any liquid water oceans and higher ice phases that may be  
127 present below, while our model rocky core represents the silicate interior. The satellite will be oblate, as  
128 it will be distorted by the degree 2 “centrifugal potential”. This is therefore a model of two nested  
129 Maclaurin spheroids. Large icy satellites have significant variation in ice density within so of course it  
130 is not our intent to use this model to obtain accurate interior models. Rather, we are using this simple  
131 model to understand the difference between exact results of a simple model and approximate (RDA)  
132 results for the same model, with and without nonhydrostatic effects.

133 In the hydrostatic limit, the two defining surfaces of the model – the surface of the body and the  
134 core-mantle boundary – will be slightly oblate due to rotation, with the magnitude of oblateness

135 directly related to the spin rate. We can define these surfaces by

$$136 \quad r_o = R[1 + \epsilon_o P_2(\cos\theta)] \quad (4a)$$

$$137 \quad r_c = R_c[1 + \epsilon_c P_2(\cos\theta)] \quad (4b)$$

138 where  $r_o$  is the radius of the satellite,  $r_c$  is the core radius,  $R_c$  is the mean core radius,  $P_2$  is the degree 2  
 139 Legendre polynomial,  $\theta$  is the colatitude, and the  $\epsilon$ 's are oblateness factors that give a measure of how  
 140 flattened the satellite and core surfaces are. The oblateness of the satellite has the effect of introducing  
 141 a degree 2 term to the external gravitational potential of the satellite, defined by

$$142 \quad V_2 = \frac{G}{r} \int \rho(\vec{r}') \left(\frac{r'}{r}\right)^2 P_2(\cos\theta) P_2(\cos\theta') d^3\vec{r}' \quad (5)$$

143 where  $r$  is the distance from the center of the satellite and  $\rho$  is the density distribution of the satellite; all  
 144 primed variables represent positions on or within the satellite. Since the two regions within the body  
 145 are of constant density and the Legendre functions are orthogonal, the only contributions to the integral  
 146 come from the deformations of the core and surface. By definition of  $J_2$ ,  $V_2 = -J_2 P_2 GMR^2/r^3$  whence  
 147 Equation 5 can be solved to yield

$$148 \quad J_2 = -\frac{3}{5} \frac{y\epsilon_o + x^5(1-y)\epsilon_c}{y + x^3(1-y)} \quad (6)$$

149 where  $x = R_c/R_o$ ,  $y = \rho_o/\rho_c$ , and we have kept terms to only first order in the  $\epsilon$ 's, as they are of the same  
 150 order as  $q$  and much less than unity for typical icy satellites.

151 To derive the  $\epsilon$ 's, we evaluate the satellite and core surfaces as equipotentials. At the satellite  
 152 surface, the relevant potentials are the degree 0 and 2 gravitational potentials and the ‘‘centrifugal  
 153 potential’’:

$$154 \quad V_{surf} = \frac{GM}{r} - \frac{GMR^2}{r^3} J_2 P_2 + \frac{1}{3} r^2 \Omega^2 (1 - P_2) \quad (7a)$$

155 where we have omitted the colatitudes dependence of  $P_2$  for simplicity. We then solve equation 7a on  
 156 the satellite surface so that

$$157 \quad V_{surf} = \frac{GM}{R} (1 - \epsilon_o P_2) - \frac{GM}{R} J_2 P_2 + \frac{1}{3} R^2 \Omega^2 (1 - P_2) \quad (7b)$$

158 where we have retained only terms that are linear in the perturbation (recall that terms such as  $\epsilon J_2$  are  
 159 second order) . To qualify as an equipotential, the surface must not have any potential variations with  
 160 latitude or longitude; thus, the summed coefficient of  $P_2$  is zero:

$$161 \quad -\frac{GM}{R}\epsilon_0 - \frac{GM}{R}J_2 - \frac{1}{3}R^2\Omega^2 = 0 \quad (7c)$$

162 . Solving for  $\epsilon_0$  and incorporating equation 3, we get

$$163 \quad \epsilon_0 = -J_2 - \frac{q}{3} \quad (7d)$$

164 Finally, plugging in equation 6 and simplifying gives:

$$165 \quad \epsilon_0 = \frac{-\frac{5q}{3}[(1-y)x^3+y]+3x^5(1-y)\epsilon_c}{2y+5x^3(1-y)} \quad (8)$$

166 Outside the core surface (but beneath the surface), the relevant potentials are the degree 0 and 2  
 167 gravitational potentials of the core, the degree 2 gravitational potential of the mantle (which can come  
 168 only from the surface distortion), and the ‘‘centrifugal potential’’:

$$169 \quad V_{core} = \frac{GM_c}{r} + \frac{4}{5}\pi Gr^2\rho_o P_2\epsilon_o + \frac{4}{5}\pi \frac{GR_c^5}{r^3}(\rho_c - \rho_o)P_2\epsilon_c + \frac{1}{3}r^2\Omega^2(1 - P_2) \quad (9)$$

170 By Gauss’ law there is no degree 0 contribution from the mantle. Evaluating at the core surface  
 171 (equation 4b), we obtain

$$172 \quad \frac{3}{5}y\epsilon_o = \frac{q_c}{3} + \frac{1}{5}\epsilon_c(2 + 3y) \quad (10)$$

173 where

$$174 \quad q_c = q[x^3(1 - y) + y] \quad (11)$$

175 Combining equations 6, 8, and 10 allows us to solve for  $J_2$  and the  $\epsilon$ ’s in terms of  $q$ ,  $x$ , and  $y$ . Finally, as  
 176 we have measured values of the total mass and mean radius of the major icy satellites, we can relate  $x$   
 177 and  $y$  by noting that

$$178 \quad M = \frac{4}{3}\pi[(\rho_c - \rho_o)R_c^3 + \rho_o R^3] \quad (12a)$$

179 which can be simplified to

180 
$$y = \frac{x^3}{\tau + x^3 - 1} \quad (12b)$$

181 where

182 
$$\tau = \frac{3M}{4\pi\rho_o R^3} \quad (12c)$$

183 is the ratio of mean satellite density to surface density.

184 The RDA assumes that the bodies in question are devoid of large density variations. To assess  
 185 this assumption, we use our simple 2-layer model and calculate its exact MOI to first order in  $q$  using

186 
$$\frac{C}{MR^2} = \frac{\int s^2 dm}{MR^2} \quad (13a)$$

187 where  $s$  is the distance between a mass element  $dm$  of the satellite and the rotation axis. Evaluating  
 188 equation 13a and simplifying using equation 6, we get

189 
$$\frac{C}{MR^2} = \frac{2}{5} \left[ \frac{x^5(1-y)+y}{x^3(1-y)+y} \right] + \frac{2}{3} J_2 \quad (13b)$$

190 where the first term represents the polar moment of inertia of a spherical body with two constant  
 191 density layers, and the second term represents the first order correction to the polar moment of inertia  
 192 due to rotation-induced oblateness. We do not include higher order terms as they are small. We can now  
 193 compare the exact MOI calculated in equation 13b with the MOI calculated using the RDA. Figure 1  
 194 shows the percentage error in the RDA-derived MOI as a function of the core and mantle densities,  
 195 constrained by Titan's mean density (which determines core radius fraction  $x$ ) and rotation rate. These  
 196 models are not attempting to fit the measured MOI but rather to assess the error in RDA for Titan-like  
 197 models. The results show that the RDA-derived MOIs are <1% different from the exact MOIs for the  
 198 range of densities of interest. The sign of the error changes in the density range of interest so it is not  
 199 consistently in one direction. We also see that the absolute errors largely increase with increasing  
 200 difference between the mantle and core densities, as expected with the assumption in question.

201 Although the error is small, it is noteworthy that there is not an exact one-to one correspondence

202 between the value of  $J_2/q$  and  $C/MR^2$ . This is evident from the fact that the equations determining the

203 true  $C/MR^2$  cannot be mapped onto equation 13b. It is indeed surprising that RDA works as well as it  
204 does since the exact formulation has so little in common with the formula used in RDA.

205         Exact results for icy satellites are also given in Zharkov et al. (1985), but they did not examine  
206 the differences with RDA in detail. Zharkov (2004) showed that the RDA-derived MOI for Io was  
207 within  $\sim 0.1\%$  of that derived from the first term of equation 13b, which is in agreement with our results  
208 since the second term of equation 13b is small in comparison. They also showed that the inclusion of  
209 second order terms in  $q$  in the RDA resulted in an order of magnitude decrease in the errors.  
210 Meanwhile, results from the comparison of RDA-derived flattening and surface eccentricity in the  
211 linear limit to that of the exact solution of Kong et al. (2010) showed errors of comparable magnitude  
212 for bodies with internal structures and rotation rates applicable to large icy satellites (Schubert et al.  
213 2011).

214         To explore all available phase space in density and core size variations, we plot in figure 2 the  
215 percent error between the exact and RDA-derived MOIs as a function of the ratio of the core radius to  
216 the total radius and the ratio of the density of the outer layer to that of the inner layer for a wider range  
217 of values than those appropriate for Titan-like bodies, though we constrain the rotation rate and radius  
218 to that of Titan's and the core density to a value of  $3 \text{ g cm}^{-3}$ . Here we see that errors  $>10\%$  are possible  
219 as the density of the outer layer becomes  $<5\%$  that of the inner layer. The white area indicates parts of  
220 the phase space where the absolute error between the exact and RDA-derived MOIs is greater than  
221  $50\%$ . Within this region, the error increases rapidly such that, at the bottom of the figure, the error  
222 reaches almost  $300\%$ . This highlights the limitations of the RDA for bodies with large, extended outer  
223 layers surrounding a dense inner layer, such as within the giant planets of both our Solar System and  
224 extrasolar planetary systems.

## 225 *2.2. Nonhydrostatic Effects and Stress*

226         In the above analysis, we assumed hydrostatic equilibrium and were thus able to solve for the

227 oblateness factors  $\epsilon_o$  and  $\epsilon_c$  by assuming the satellite and core surfaces were equipotentials. In the case  
 228 where nonhydrostatic effects are present however, these surfaces would no longer be equipotentials and  
 229 we then assume that the  $\epsilon$ 's could be slightly different values. To quantify this effect, we assume that  
 230 the deviations of the  $\epsilon$ 's from their hydrostatic values are small, and thus we can Taylor expand the  
 231 RDA around the hydrostatic value of  $\Lambda_{2,0}$ , which is directly proportional to  $J_2$ , which is in turn directly  
 232 proportional to the  $\epsilon$ 's. In other words, if we let  $C/MR^2 = f(\Lambda_{2,0})$ , where  $f$  is the right hand side of  
 233 equation 2, then

$$234 \quad f(\Lambda_{2,0}^{nh}) - f(\Lambda_{2,0}^h) = \left( \frac{df}{d\Lambda_{2,0}} \right)_{\Lambda_{2,0}^h} \frac{(a\Delta\epsilon_o + b\Delta\epsilon_c)}{q} \quad (14a)$$

235 where the nh and h superscripts denote nonhydrostatic and hydrostatic values, respectively;  $\Delta\epsilon_z = \epsilon_z^{nh} -$   
 236  $\epsilon_z^h$ ,  $z = o, c$ ;  $a$  and  $b$  are given by

$$237 \quad a = -\frac{3}{5} \frac{y}{y + x^3(1-y)} \quad (14b)$$

$$238 \quad b = -\frac{3}{5} \frac{x^5(1-y)}{y + x^3(1-y)} \quad (14c)$$

239 and

$$240 \quad \frac{df}{d\Lambda_{2,0}} = 2 \left( \frac{5}{3\Lambda_{2,0} + 1} - 1 \right)^{-1/2} (3\Lambda_{2,0} + 1)^{-2} \quad (14d)$$

241 For the parameters of interest to us, this derivative is  $\sim 0.4$ . Since  $C/MR^2$  and  $\Lambda_{2,0}$  are both about 1/3 for  
 242 Titan-like models, this means that a 2.5% difference between  $\Lambda_{2,0}^h$  and  $\Lambda_{2,0}^{nh}$  will lead to a 1% error in  
 243  $C/MR^2$ . Note that we are treating the nonhydrostatic distortions as independent variables but the reality  
 244 could be more complicated. For example, if one assumed that the core surface was nonhydrostatic but  
 245 the outer surface was still hydrostatic then the hydrostatic surface shape would necessarily change (by  
 246 equation 7d). This is indeed an interesting case since the core (being rock) is more likely to be  
 247 nonhydrostatic than the shell. In this particular instance, equation 8 tells us that

$$248 \quad \Delta\epsilon_o = \frac{3x^5(1-y)\Delta\epsilon_c}{2y + 5x^3(1-y)} \quad (15a)$$

249 so that  $a\Delta\epsilon_0 + b\Delta\epsilon_c$  then becomes simply  $b^*\Delta\epsilon_c$  where

$$250 \quad \frac{b^*}{b} = 5 \left[ \frac{y+x^3(1-y)}{2y+5x^3(1-y)} \right] \quad (15b)$$

251 This exceeds unity but not greatly so for typical parameter values, and is not therefore a major issue in  
252 our simple assessment.

253 Any deviation from hydrostatic equilibrium will have an associated deviatoric stress. This stress  
254 could arise in a variety of ways: It could be elastic or it could be viscous or it could be some other more  
255 complicated rheological response. In the real body (as distinct from our idealized model) it can arise  
256 from density gradients within the material arising from compositional or thermal differences and it may  
257 vary spatially in a way that depends on the spatial variability of the rheological parameters (e.g., as in a  
258 lithosphere over a viscous substratum, a common model for icy satellites). The precise form of the  
259 deviatoric stress field for a realistic model is beyond the intent of this paper. Instead, for our idealized  
260 model, we will define the deviatoric stress as the difference between the hydrostatic stress in the  
261 presence of the nonhydrostatic structure and the hydrostatic stress in the absence of such a structure,  
262 where the hydrostatic stress is defined simply as the weight of the overlying material divided by the  
263 area. In other words, the stresses are given by the pressure changes caused by the extra mass associated  
264 with the distortion of core or shell:

$$265 \quad \sigma_o = \rho_o g_o \Delta\epsilon_o R \quad (16a)$$

$$266 \quad \sigma_c = (\rho_c - \rho_o) g_c \Delta\epsilon_c R_c \quad (16b)$$

267 for the satellite and core surfaces, respectively, where  $g_o$  is the gravitational acceleration at the satellite  
268 surface calculated by  $GM/R^2$ , and  $g_c$  is the gravitational acceleration at the core surface, given by

$$269 \quad g_c = \frac{g_o}{x^2(1-y)+y/x} \quad (17)$$

270 The actual stress field is of course a tensor so these are not the actual stresses but merely a  
271 characteristic scale for these stresses. We note, however, that in the context of viscous relaxation of a  
272 homogeneous medium, these values are indeed the order of magnitude of the driving stresses that are

273 responsible for the gradual decay of the nonhydrostatic deformations over long timescales. They are  
274 also the order of magnitude for the purely elastic stresses that would result in a uniformly elastic body.  
275 They are not the stresses that are present for a body with a more complicated, more realistic structure.  
276 For example, a thin elastic shell over a viscous interior can develop hoop stresses in the shell that are  
277 larger than the radial stress by as much as the ratio of the radius to the shell thickness. This situation  
278 can arise when a body is changing its spin state over billions of years. In those cases the stress that is  
279 needed to support the distortion of the shell away from current hydrostatic equilibrium can be much  
280 larger than the estimate provided in equation 16a. This would not apply to equation 16b and rocky core  
281 deformations, as the core is likely one large mass without any thin elastic outer shells.

282         Since  $\varepsilon \propto q = \Omega^2 R^2 / gR$  and  $\Delta\varepsilon \sim \sigma / \rho gR$ , it follows that  $\Delta\varepsilon / \varepsilon \sim \sigma / \rho \Omega^2 R^2$  is the appropriate  
283 dimensionless number characterizing the importance of nonhydrostatic effects. Evidently,  
284 nonhydrostatic effects are of greatest concern for small or slowly rotating bodies. We can now apply  
285 this model to Titan, Ganymede, Ganymede, and Enceladus to evaluate the effect of realistically  
286 supportable nonhydrostatic structures on their determined MOIs.

287

### 288 **3. RESULTS AND DISCUSSION**

289         Figure 3 shows the percent errors in the RDA-derived MOIs of Titan, Ganymede, Callisto and  
290 Enceladus caused by degree 2 nonhydrostatic structures related to the amount of stress these structures  
291 would apply on these satellites' surfaces and their cores. We see that the nominal stresses corresponding  
292 to a 10% error in the determined MOIs for Titan and Callisto are on the order of 0.1 bars for surface  
293 stresses and 1 bar for core stresses, while for Ganymede they are on the order of 1 bar for surface  
294 stresses and 10 bars for core stresses. For Enceladus, a surface stress of 0.1 bars is also enough to cause  
295 a MOI error of 10%, while core stresses of a few bars is necessary to cause the same error. This  
296 similarity in behavior arises because Enceladus's faster rotation is compensating for its lower gravity.

297 These results are consistent with our previous reasoning that faster rotators and larger bodies will  
298 require greater nonhydrostatic deviations to produce the same MOI errors as slower rotators and  
299 smaller bodies, as a nonhydrostatic structure on a fast rotating/large body would contribute a smaller  
300 fraction to the total  $J_2$ . We have fixed  $\rho_o$  and  $\rho_c$  to  $1 \text{ g cm}^{-3}$  and  $3 \text{ g cm}^{-3}$ , respectively, in our results, but  
301 they are not much changed by other choices of core and shell density and thickness.

302 Deviatoric stresses of order bars are perfectly reasonable for a silicate core. By comparison,  
303 Earth's Moon is thought to exhibit a fossil tidal bulge that imposes nonhydrostatic stresses of order tens  
304 of bars, which has survived for billions of years (Lambeck and Pullan 1980). Similar origins for any  
305 deformations within icy satellites cannot be ruled out given their poorly constrained tidal histories.  
306 Stresses of order bars are also potentially supportable in the outer regions of the icy shell or throughout  
307 the shell by thermal convection, which has been suggested to occur on Titan (Tobie et al. 2006) and  
308 Callisto and Ganymede (McKinnon 1997; 2006).

309 We turn now to the question of whether these nonhydrostatic effects could be permitted by or  
310 supported by the data. Two approaches can be made to this question. One is to appeal to observation  
311 that the observed  $J_2/C_{22}$  is close to  $10/3$ . The other is to appeal to the smallness of higher order  
312 harmonics. Both of these arguments are best considered for the Titan data where there have been  
313 sufficient flybys to assess the power present in higher order harmonics and precisely determine  $J_2/C_{22}$ .

314 We first note that the  $10/3$  value is the expected result for any rheological model in which the  
315 material parameters depend at most on the radial variable. It is thus consistent with (but does not  
316 require) a hydrostatic body. However, our main interest here is to assess small deviations away from  
317  $10/3$ . Give the definitions of  $J_2$  and  $C_{22}$  in equations 1a and 1b, let  $\alpha$  be the ratio of the prolate distortion  
318 along the satellite-planet direction to the oblate distortion (polar flattening)  $(B-A)/(C-B)$ . Then

319 
$$\frac{J_2}{C_{22}} = 2 + \frac{4}{\alpha} \quad (18)$$

320 and the case of a synchronously rotating hydrostatic satellite is  $\alpha=3$ . In general, we can write

321 
$$J_2 = J_{2,h} + J_{2,nh} \quad (19a)$$

322 
$$C_{22} = C_{22,h} + C_{22,nh} \quad (19b)$$

323 where again h means hydrostatic and nh means nonhydrostatic. We can likewise identify the  
 324 nonhydrostatic and hydrostatic contributions to A, B and C. If the observed gravity field has no other  
 325 contributions at degree 2 (i.e.,  $C_{21}$ ,  $S_{21}$ ,  $S_{22}$  are all zero) then the body is at its lowest energy state under  
 326 the action of tides and rotation. Consider now the case where the body reorients to its lowest energy  
 327 state by True Polar Wander. This means that the “permanent” rotational and tidal bulges are allowed to  
 328 be established in accordance with the orientation of the body in space (i.e., they do not follow the  
 329 reorientation) while the nonhydrostatic part is permitted to rotate into the lowest energy state. This  
 330 guarantees that  $J_{2,nh}$  and  $C_{22,nh}$  are positive and are the only non-zero components of the degree two  
 331 field. Application of RDA to the total measured  $J_2$  or  $C_{22}$  is then guaranteed to give an overestimate to  
 332 the MOI. We can attribute an  $\alpha$  value (eq. 18) to the nonhydrostatic part alone. If we write  $C_{22,nh} =$   
 333  $\delta C_{22,h}$  where  $0 < \delta \ll 1$  then it follows that

334 
$$\frac{J_2}{C_{22}} = \frac{J_{2,h} + J_{2,nh}}{C_{22,h} + C_{22,nh}} = \frac{\frac{10}{3} + \left(2 + \frac{4}{\alpha}\right)\delta}{1 + \delta} \quad (20a)$$

335 whence

336 
$$\frac{J_2}{C_{22}} \approx \frac{10}{3} \left[ 1 + \left( \frac{6}{\alpha} - 2 \right) \frac{\delta}{5} \right] \quad (20b)$$

337 As expected, this ratio is exactly 10/3 if  $\alpha = 3$ . But the deviation from 10/3 is not large even for other  
 338 values of  $\alpha$ . Consider the case of a Titan model where RDA gives  $C/MR^2 = 0.34$  (cf. Iess et al, 2010).  
 339 Suppose the true value is 0.33, i.e., different by ~3%. From equation 14d and replacing  $\Lambda_{2,0}$  by  
 340  $4C_{22}/3q$ , we know that this can arise from a nonhydrostatic correction of 7.5% in  $C_{22}$ . Setting  $\delta = 0.075$ ,  
 341 we find that  $J_2/C_{22}$  deviates from 10/3 by  $5(3/\alpha - 1)\%$ . We do not know the value of  $\alpha$ , but any value  
 342 larger than 1.5 yields an error of 5% or less. Table 1 of Iess et al. (2010) does not exclude a deviation of  
 343 5% (recall that one sigma error bars are quoted). This should not be confused with the formal error in

344  $C_{22}$  which is indeed much smaller. A similar result applies irrespective of how the nonhydrostatic  
345 correction is apportioned between  $J_2$  and  $C_{22}$ . Accordingly, the data do not exclude a  $C/MR^2$  of 0.33.  
346 This value is at the upper end of possible values for a fully differentiated Titan (Castillo-Rogez and  
347 Lunine, 2010).

348         Alternatively, we could estimate nonhydrostatic effects by assuming that the power in higher  
349 harmonics is an indication of power in the nonhydrostatic degree 2. From Iess et al. (2010) we see that  
350 the degree three harmonics are as large as 5% of degree 2 (but with large uncertainty). This is similar to  
351 the example offered above and is therefore consistent with our conclusion about a possible 3% error in  
352  $C/MR^2$ . This argument is based on a possibly incorrect assumption since the physical source of degree  
353 2 nonhydrostaticity might contribute nothing at degree 3. A possible case of interest is a shape that  
354 “froze in” at a time when the satellite was closer to the planet. This would give a false high MOI if  
355 RDA were applied. Yet another case, probably of importance for Titan is a nonhydrostatic contribution  
356 arising from tidal heating (Nimmo and Bills, 2010). This would also be expected to give positive  
357 contributions to the harmonics and therefore yield a higher RDA-derived MOI than the true value.

358         In the case of Ganymede there were only two flybys and this prevented a reliable determination  
359 of higher harmonics (Anderson et al, 2004). However there is no doubt that higher harmonics are  
360 needed to describe the data. This led to an analysis based on mass anomalies (Palguta et al, 2006) but  
361 insufficient information to perform the analysis we provide here for Titan. In the case of Callisto, there  
362 is insufficient data to assess the magnitude of nonhydrostatic effects. Evidently, we require larger  
363 nonhydrostaticity for Callisto than is observed for Titan in order to have that body be as differentiated  
364 as Titan. It is not even possible to exclude a Ganymede-like MOI for Callisto.

365

#### 366 **4. SUMMARY AND CONCLUSIONS**

367         The primary method for the determination of the internal structures of large icy satellites in our

368 Solar System is the estimation of their moments of inertia (MOI) via the Radau-Darwin Approximation  
369 (RDA), which assumes a homogeneous interior in hydrostatic equilibrium. However, these assumptions  
370 are challenged by the gravity measurements of Titan, Ganymede, and Callisto, which show these  
371 bodies to be at least partially differentiated with clear signals of nonhydrostatic structures. In order to  
372 determine the validity of these assumptions, we constructed a simple hydrostatic 2-layer icy satellite  
373 model and determined its degree 2 gravity coefficient  $J_2$ , which is necessary in the use of the RDA. We  
374 showed that in the hydrostatic limit the RDA is valid to within 99% for most configurations of core size  
375 and internal density variations, including those applicable to all solid bodies in the Solar System. Errors  
376 in RDA become  $>10\%$  when the outer layer becomes  $<5\%$  as dense as the inner layer, which represents  
377 bodies like the gas giants.

378 To introduce nonhydrostatic effects, we altered the oblateness of the model to nonhydrostatic  
379 shapes and calculated the resulting  $J_2$ 's. This in turn allowed us to relate the change in the RDA-derived  
380 MOIs to the changes in the magnitude of the nonhydrostatic effects and thus calculate the errors  
381 between the RDA-derived MOIs and the true MOIs of the model due to nonhydrostatic effects. We also  
382 calculated the stresses applied to the model by these nonhydrostatic features to evaluate the validity of  
383 the MOI errors. We then applied our calculations to Titan, Ganymede, and Callisto. We showed that the  
384 RDA-derived MOIs of Titan and Callisto can be  $\sim 10\%$  greater than the actual MOIs given  
385 nonhydrostatic stresses of  $\sim 0.1$  bars on the surface or  $\sim 1$  bar on the core surface; for Ganymede, these  
386 two values are an order of magnitude greater. We also applied our calculations to Enceladus, and  
387 showed that an MOI error of 10% is possible given nonhydrostatic stresses of  $\sim 0.1$  bars on the surface  
388 and a few bars on the core surface. These results are largely independent of the model parameters used,  
389 such as the density of the two layers and the core size. We conclude that the RDA-derived MOIs of  
390 slow-rotators and small bodies such as Titan, Callisto, and Enceladus are most affected by  
391 nonhydrostatic structures, while faster rotators and/or larger bodies like Ganymede are less affected.

392 This is especially important for future analysis of Enceladus gravity measurements in determining its  
393 MOI given the large nonhydrostatic contribution from its southern polar depression.

394 The nonhydrostatic structures corresponding to the aforementioned stresses have not been ruled  
395 out in the case of Titan given recent gravity measurements from Cassini, while data for Ganymede,  
396 Callisto, and Enceladus are insufficient to provide any bounds on the degree of nonhydrostatic  
397 structures present. Therefore, the difference in the observed MOIs of Titan/Callisto and Ganymede –  
398 and thus the perceived dichotomy of their internal structures – may be entirely due to nonhydrostatic  
399 effects, and that it is possible all three bodies are fully differentiated.

400 Our work shows that caution must be exercised in determining the MOIs of the outer Solar  
401 System icy satellites using the RDA, and that the nonhydrostatic contributions to their gravity fields  
402 must be better characterized if we are to rely on their MOIs to construct models of their interior  
403 structures, their formation, and their evolution.

404 **REFERENCES**

- 405  
406 Anderson J. D., Lau E. L., Sjogren W. L., Schubert G., and Moore W. B. (1996) Gravitational  
407 constraints on the interior structure of Ganymede. *Nature*, 384, pp. 541-543.  
408  
409 Anderson J. D., Jacobson R. A., McElrath T. P., Moore W. B., Schubert G., Thomas P. C. (2001) Shape,  
410 mean radius, gravity field, and internal structure of Callisto. *Icarus*, 153, pp. 157-161.  
411  
412 Anderson, J.D., Schubert, G., Jacobson, R.A., Lau, E.L., Moore, W.B., Palguta, J., 2004.  
413 Discovery of mass anomalies on Ganymede. *Science* 305, 989–991.  
414  
415 Barr A. C. and Canup R. M. (2008) Constraints on gas giant satellite formation from the interior states  
416 of partially differentiated satellites. *Icarus*, 198, pp. 163-177.  
417  
418 Barr A. C., Citron R. I., and Canup R. M. (2010) Origin of a partially differentiated Titan. *Icarus*, 209,  
419 pp. 858-862.  
420  
421 Canup R. M. and Ward W. R. (2002) Formation of the Galilean satellites: conditions of accretion.  
422 *Astron. J.*, 124, pp. 3404-3424  
423  
424 Castillo-Rogez J. C. and Lunine J. I. (2010) Evolution of Titan’s rocky core constrained by Cassini  
425 observations. *Geophys. Res. Lett.*, 37, L20205, 5pp.  
426  
427 Fortes A. D. (2012) Titan’s internal structure and the evolutionary consequences. *Planet. Space. Sci.*,  
428 60, pp. 10-17.  
429  
430 Hubbard W. B. (1984) In: *Planetary Interiors*. Von Nostrand Reinhold Company Inc., New York, New  
431 York, USA.  
432  
433 Hubbard W. B. (2012) High-precision Maclaurin-based models of rotating liquid planets. *Astrophys. J.*  
434 *Lett.*, 756, L15, 3pp.  
435  
436 Iess L., Rappaport N. J., Tortora P., Lunine J., Armstrong J. W., Asmar S. W., Somenzi L., and Zingoni  
437 F. (2007) Gravity field and interior of Rhea from Cassini data analysis. *Icarus*, 190, pp. 585-593.  
438  
439 Iess L., Rappaport N. J., Jacobson R. A., Racioppa P., Stevenson D. J., Tortora P., Armstrong J. W., and  
440 Asmar S. W. (2010) Gravity field, shape, and moment of inertia of Titan. *Science*, 327, pp. 1367-1369.  
441  
442 Jacobson R. A., Antreasian P. G., Bordi J. J., Criddle K. E., Ionasescu R., Jones J. B., Mackenzie R. A.,  
443 Meek M. C., Parcher D., Pelletier F. J., Owen W. M. Jr., Roth D. C., Roundhill I. M., and Stauch J. R.  
444 (2006) The gravity field of the Saturnian system from satellite observations and spacecraft tracking  
445 data. *Astron. J.*, 132, pp. 2520-2526.  
446  
447 Kong D., Zhang K., and Schubert G. (2010) Shapes of two-layer models of rotating planets. *J.*  
448 *Geophys. Res.*, 115, E12003, 11pp.  
449  
450 Lambeck K. and Pullan S. (1980) The lunar fossil bulge hypothesis revisited. *Phys. Earth Planet. In.*,  
451 22, pp. 29-35.

452  
453 McKinnon W. B. (1997) Mystery of Callisto: Is it undifferentiated? *Icarus*, 130, pp. 540-543.  
454  
455 McKinnon W. B. (2006) On convection in ice I shells of outer Solar System bodies, with detailed  
456 application to Callisto. *Icarus*, 183, pp. 435-450.  
457  
458 Mosqueira I. and Estrada P. R. (2003) Formation of the regular satellites of giant planets in an extended  
459 gaseous nebula I: subnebula model and accretion of satellites. *Icarus*, 163, pp. 198-231.  
460  
461 Mueller S. and McKinnon W. B. (1988) Three-layered models of Ganymede and Callisto:  
462 compositions, structures, and aspects of evolution. *Icarus*, 76, pp. 437-464.  
463  
464 Murray C. D. and Dermott S. F. (1999) In: *Solar System Dynamics*. Cambridge University Press, New  
465 York, New York, USA.  
466  
467 Nimmo F. and Bills B. G. (2010) Shell thickness variations and the long-wave topography of Titan.  
468 *Icarus*, 208, pp. 896-904.  
469  
470 O'Rourke J. and Stevenson D. J. (2013) Stability of ice/rock mixtures with application to a partially  
471 differentiated Titan. *Icarus*, in revision.  
472  
473 Palguta J., Anderson J. D., Schubert G., and Moore W. B. (2006) Mass anomalies on Ganymede.  
474 *Icarus*, 180, pp. 428-441.  
475  
476 Schubert G., Anderson J., Zhang K., Kong D., and Helled R. (2011) Shapes and gravitational fields of  
477 rotating two-layer Maclaurin ellipsoids: Application to planets and satellites. *Phys. Earth Planet. In.*,  
478 187, pp. 364-379.  
479  
480 Showman A. P. and Malhotra R. (1999) The Galilean satellites. *Science*, 286, pp. 77-84.  
481  
482 Stevenson D. J. (2001) Jupiter and its moons. *Science*, 294, pp. 71-72.  
483  
484 Tobie G., Lunine J. I., and Sotin C. (2006) Episodic outgassing as the origin of atmospheric methane on  
485 Titan. *Nature*, 440, pp. 61-64.  
486  
487 Zharkov V., Leontjev, V.V. and Kozenko, A. V. (1985) Models, Figures and Gravitational Moments of  
488 the Galilean satellites of Jupiter and Icy Satellites of Saturn. *Icarus* 61, 92-100.  
489  
490 Zharkov V. N. (2004) A theory of the equilibrium figure and gravitational field of the Galilean satellite  
491 Io: The second approximation. *Astron. Lett+*, 30, pp. 496-507.

	<b>Titan</b>	<b>Ganymede</b>	<b>Callisto</b>	<b>Enceladus</b>
<b>Mass (<math>10^{26}</math> g)</b>	$1.3452 \pm 0.0002^c$	$1.48167 \pm 0.0002^d$	$1.0759 \pm 0.0001^e$	$0.00108 \pm 1e-6^c$
<b>Mean Radius (km)</b>	$2574.73 \pm 0.09^f$	$2634.1 \pm 0.3^g$	$2408.4 \pm 0.3^g$	$252.1 \pm 0.1^c$
<b>Orbital Period (Earth days)<sup>a</sup></b>	$15.95^h$	$7.15^h$	$16.69^h$	$1.37^h$
<b>MOI<sup>b</sup></b>	$0.3414 \pm 0.0005^f$	$0.3105 \pm 0.0028^d$	$0.3549 \pm 0.0042^e$	Unknown
<b>q (<math>10^{-5}</math>)<sup>i</sup></b>	3.9545	19.131	3.6958	626.374

492

493 <sup>a</sup> Assumed to be the same as rotation period, i.e. synchronous rotation.

494 <sup>b</sup> Moment of inertia in units of  $C/MR^2$ , where C, M, and R are the polar moment of inertia, mass, and  
495 mean radius of the body in question.

496 <sup>c</sup> Jacobson et al. 2006.

497 <sup>d</sup> Anderson et al. 1996.

498 <sup>e</sup> Anderson et al. 2001. Callisto mass and associated uncertainty calculated from dividing given GM  
499 value and GM uncertainty by given G value.

500 <sup>f</sup> Iess et al. 2010 (SOL1 flybys)

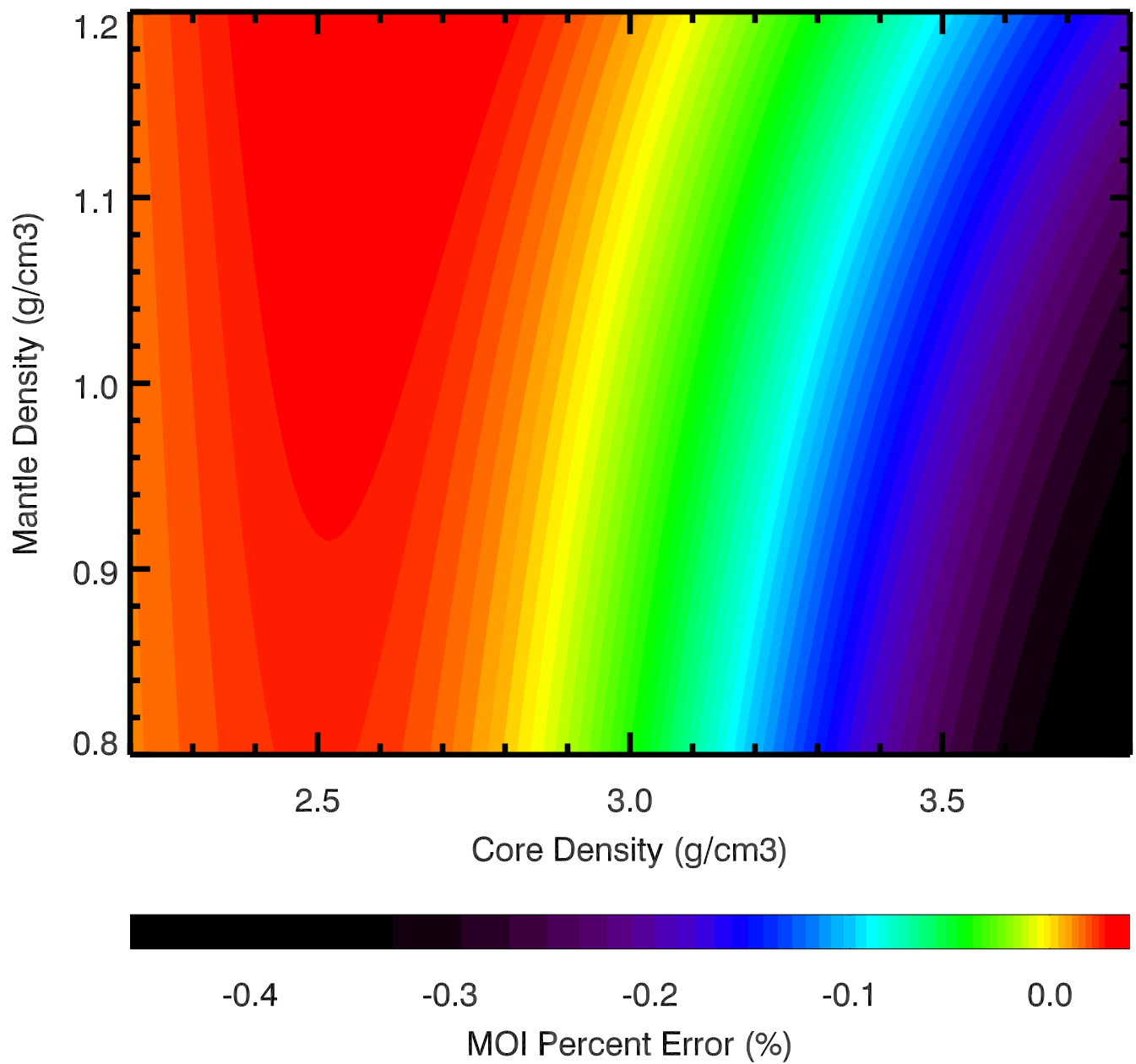
501 <sup>g</sup> Showman and Malhotra 1999.

502 <sup>h</sup> Murray and Dermott 1999 (no uncertainties were given).

503 <sup>i</sup>  $q = \Omega^2 R^3 / GM$ , where  $\Omega$ , R, and M are the spin/orbital angular velocity, radius, and mass, respectively,  
504 of the satellite; and G is the gravitational constant.

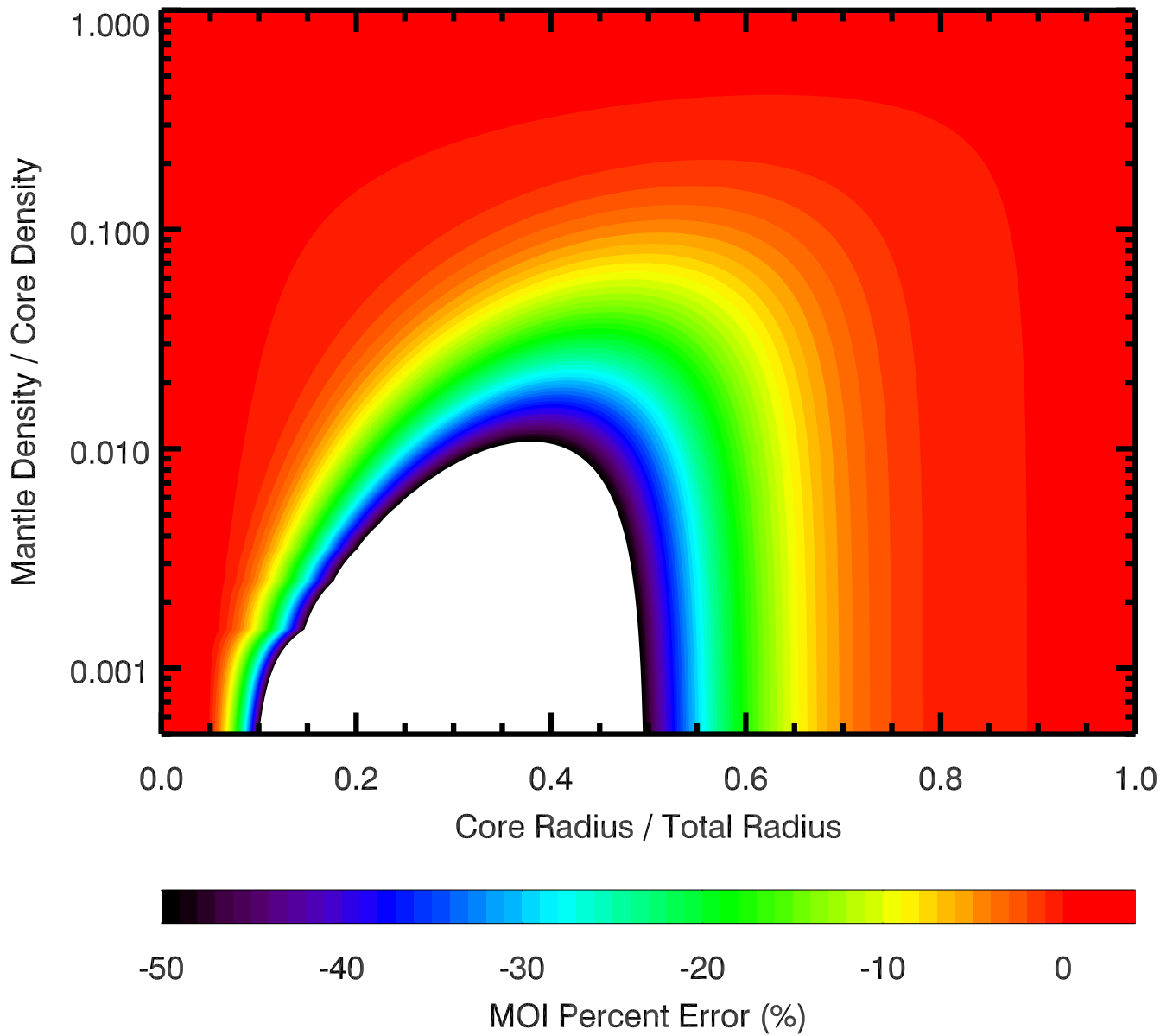
505

506 Table 1. Selected physical and orbital parameters of Titan, Ganymede, Callisto, and Enceladus.



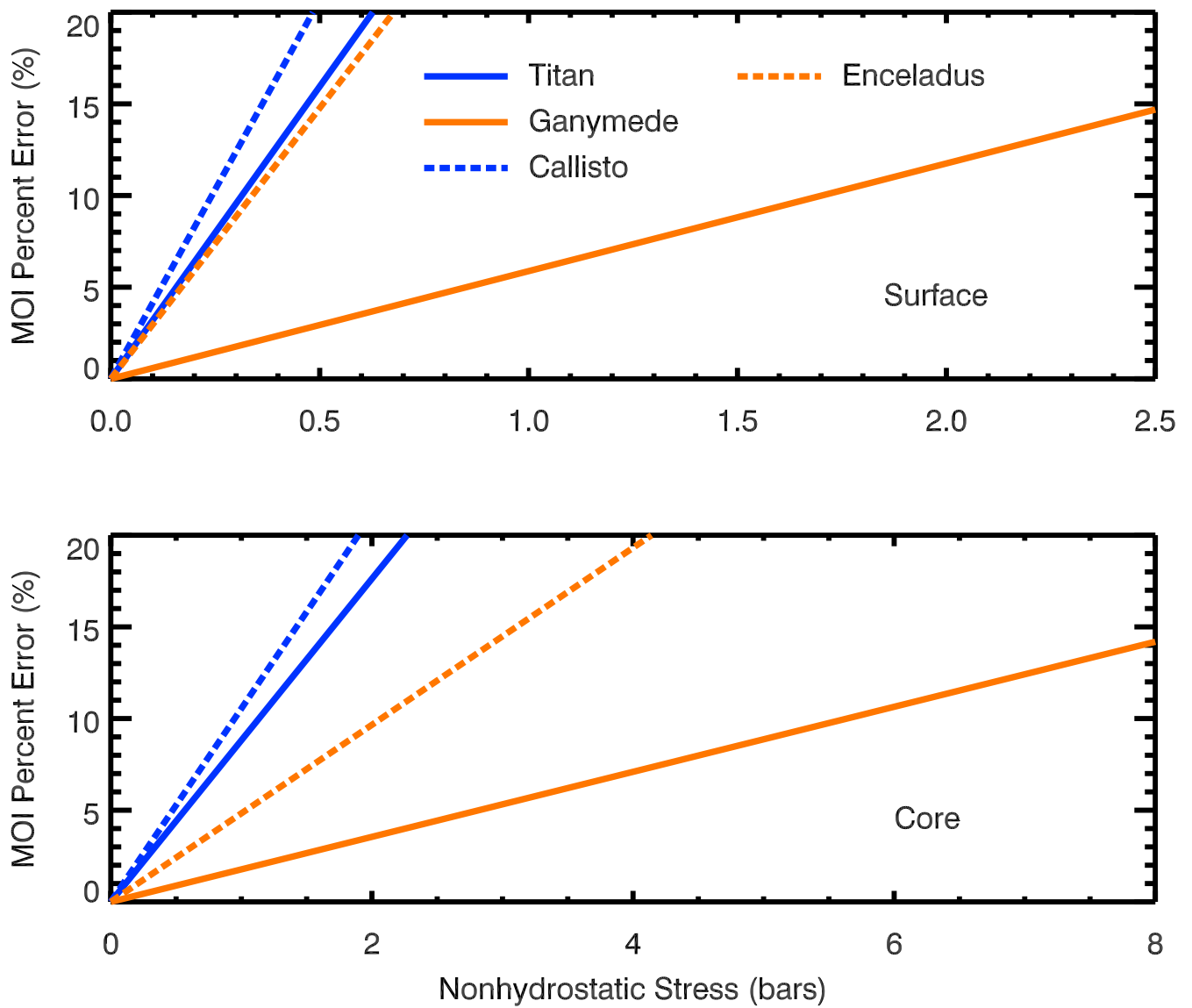
507  
 508  
 509  
 510  
 511  
 512  
 513

Figure 1. The percent error between the true moment of inertia of a hydrostatic 2-layer icy satellite calculated to first order in  $q$  and one calculated by the Radau Darwin Approximation as a function of the mantle and core densities. The model is constrained by the density and rotation rate of Titan.



514  
 515  
 516  
 517  
 518  
 519  
 520  
 521  
 522  
 523  
 524

Figure 2. The percent error between the true moment of inertia of a hydrostatic 2-layer oblate body calculated to first order in  $q$  and one calculated by the Radau Darwin Approximation as a function of the core radius to total radius ratio, and the outer layer density to inner layer density ratio. The model is constrained by the radius and rotation rate of Titan and a density of  $3 \text{ g cm}^{-3}$  for the core. The white area in the lower left represents all percent error values below  $-50\%$ , with a maximum absolute error within the range of the plot of  $\sim 293\%$ . The y axis is in log scale to emphasize the increase in percent error as the ratio of the layers' densities approaches zero.



525  
526

527 Figure 3. The percent error in the moment of inertia calculated by the Radau Darwin Approximation for  
 528 Titan, Ganymede, Callisto, and Enceladus due to a degree 2 nonhydrostatic structure on the satellite  
 529 surface (top) and core mantle boundary (bottom), as a function of the stress imparted by such a  
 530 structure on the satellite.